Morphology-Dependent Phase Selectivity of Cobalt Sulfide during Nanoparticle Cation Exchange Reactions

Auston G. Butterfield,[1] Connor R. McCormick,[1,‡] Joseph M. Veglak,[1,‡] Raymond E. Schaak[1,2,3,*]

[1] Department of Chemistry, [2] Department of Chemical Engineering, and [3] Materials Research Institute, The Pennsylvania State University, University Park, PA 16802, USA

ABSTRACT: Achieving phase selectivity during nanoparticle synthesis is important because crystal structure and composition influence reactivity, growth, and properties. Cation exchange provides a pathway for targeting desired phases by modifying composition while maintaining crystal structure. However, our understanding of how to selectively target different phases in the same system is limited. Here, we demonstrate morphology-dependent phase selectivity for wurtzite (wz) CoS, which is hcp, *vs* pentlandite Co_9S_8, which is ccp, during Co^{2+} exchange of roxbyite $Cu_{1.8}S$ plates, spheres, and rods. The plates form wz-CoS, the spheres form both wz-CoS and Co_9S_8, and the rods form Co_9S_8. The plates, spheres, and rods have nearly identical widths but increase in length in the direction that the close-packed planes stack, which influences the ability of the anions to shift from hcp to ccp during cation exchange. This morphology-dependent behavior, which correlates with the number of stacked close-packed planes, relies on an anion sublattice rearrangement that is concomitant with cation exchange, thereby providing a unique pathway by which crystal structure can be controlled and phase selectivity can be achieved during nanocrystal cation exchange.

Cation exchange is a powerful post-synthetic modification strategy that changes the composition of a nanoparticle while maintaining its morphology and, in many cases, crystal structure.[1–4] Common examples involve exchanging the Cu^+ cations in roxbyite $Cu_{1.8}S$ with Zn^{2+} or Cd^{2+}.[5–8] In these and related systems, the distorted hexagonally close packed (hcp) sulfur sublattice of roxbyite is retained to produce wurtzite-type phases, but these are generally not the thermodynamically preferred structures.[7, 9–10] Cation exchange therefore provides a reaction framework for targeting the formation of phases that are not readily accessible through direct synthetic methods.

Understanding when and why crystal structure is and is not retained during nanoparticle cation exchange is fundamental to being able to target a desired phase and for designing nanostructures with precise control over their key features. Crystal structure is generally retained when the incoming and outgoing cations are comparable in size.[6–7,11–12] Volume changes are minimized and the crystallographic site preferences, based on cation:anion radius ratios and coordination environments, are maintained. Crystal structure is usually *not* retained when there is a significant size mismatch between the outgoing and incoming cations, where a large volume change helps facilitate anion sublattice rearrangement.[1,13–15] Chemically-triggered anion sublattice changes can also occur, such as when trioctylphosphine (TOP) extracts sulfur to change the composition and phase, but these are generally decoupled from the cation exchange step.[5,12,16–18]

Cobalt sulfide provides an instructive system for interrogating phase selectivity during cation exchange. Starting with roxbyite $Cu_{1.8}S$ plates, exchanging the Cu^+ cations with Co^{2+} produces wurtzite CoS (wz-CoS).[10] This is significant, because wz-CoS is not a thermodynamically stable Co–S phase. The thermodynamically stable Co–S phase that is closest to 1:1 Co:S is Co_9S_8 (pentlandite), which differs from wz-CoS in both anion and cation sublattice structure (Figure 1).[19] The sulfur anions in wz-CoS are hcp, while in Co_9S_8 they are ccp. The cobalt cations in wz-CoS are tetrahedrally coordinated, while those in Co_9S_8 are both tetrahedral and octahedral, with sufficiently close Co–Co contacts in the tetrahedral sites to facilitate metallic bonding.[20] Here, we demonstrate that the formation of wz-CoS *vs* Co_9S_8 during cation exchange is morphology-dependent. We rationalize this behavior by considering how the various morphologies influence the anion sublattice rearrangement from hcp to ccp that is required for phase selectivity.

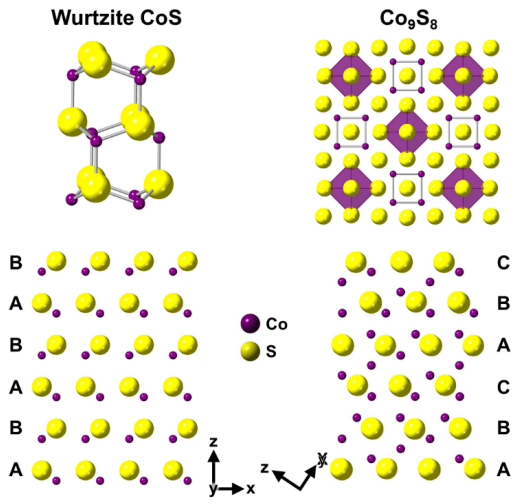

Figure 1. Crystal structures and stacking sequences of wurtzite CoS (hcp) and Co_9S_8 (ccp).

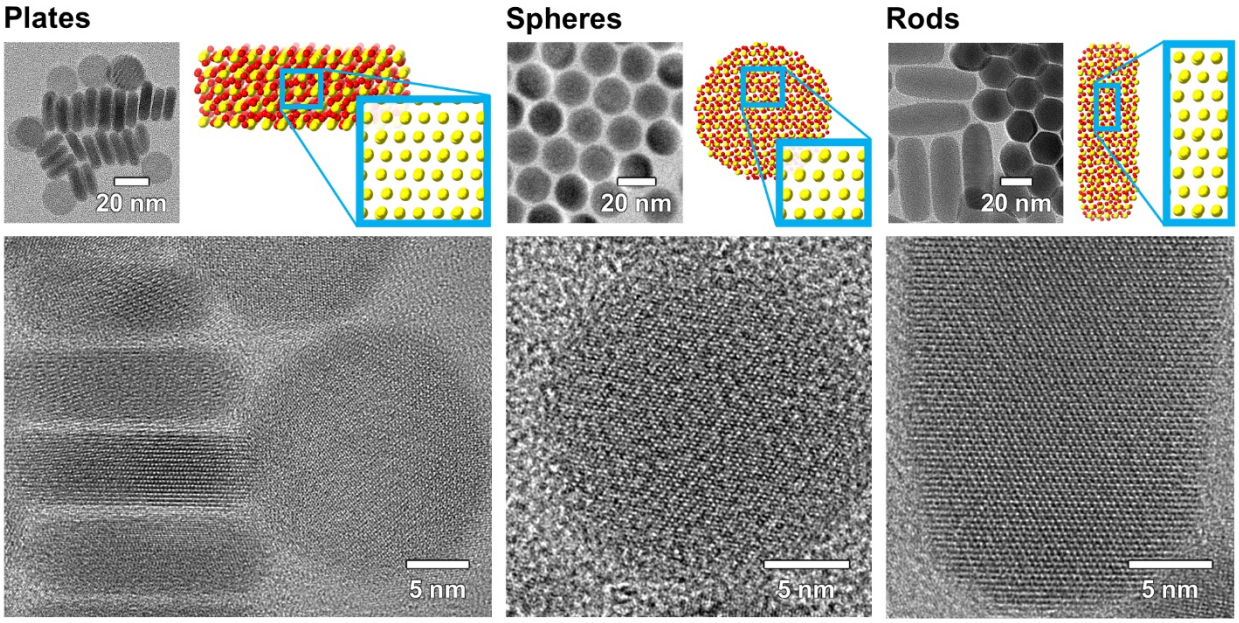

Figure 2. TEM and HRTEM images of roxbyite $Cu_{1.8}S$ plates, spheres, and rods, along with crystal structure depictions highlighting the corresponding stacking directions of the distorted hcp close packed planes.

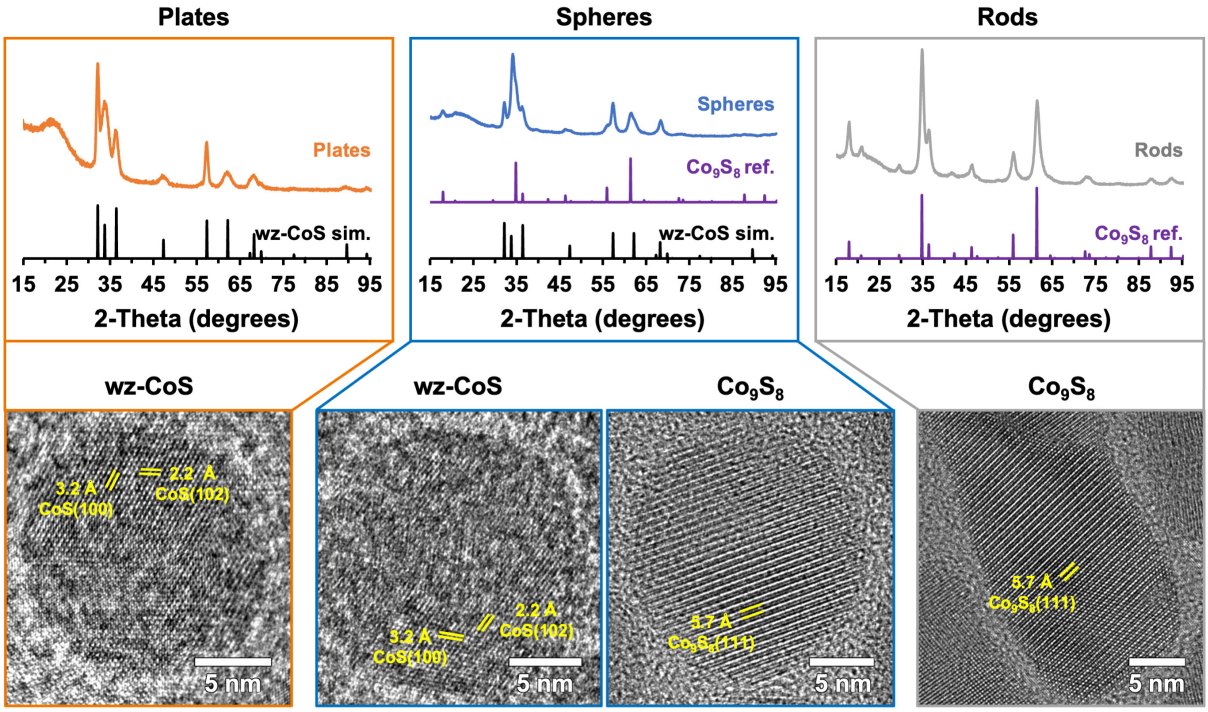

Figure 3. Top: XRD patterns for Co-S nanocrystals formed through Co^{2+} exchange of $Cu_{1.8}S$ plates, spheres, and rods. Reference patterns for wz-CoS[10] and Co_9S_8 (PDF 04-006-5681) are shown for comparison. Bottom: Corresponding HRTEM images for each product observed for each morphology.

We began by synthesizing roxbyite $Cu_{1.8}S$ nanoparticles as plates, spheres, and rods.[6,10,21] TEM and HRTEM images for each morphology are shown in Figure 2; XRD data are shown in Figure S1 of the Supporting Information. Structural representations of the anion sublattices are also shown in Figure 2. In the plane of the close-packed layers, each morphology has approximately the same diameters: plates = 18±2 nm, spheres = 18±1 nm, and rods = 19±1 nm. Despite having similar ~18-nm diameters, each morphology differs in length along the direction corresponding to the stacking of the close-packed layers – plates = 6±1 nm, spheres = 18±1 nm, and rods = 54±2 nm – making it the most important dimension when considering rearrangements between hcp and ccp.

We performed Co^{2+} exchange, as described in detail in the Supporting Information, on the $Cu_{1.8}S$ plates, spheres, and rods at temperatures ranging from 70 ºC (the minimum

temperature at which complete exchange was observed) to 140 ºC (above which, TOP-induced etching occurs more readily). We first consider the results of cation exchange at 70 ºC (Figure 3). For the plates, Co^{2+} exchange produced wz-CoS, retaining crystal structure as expected.[10] For the spheres, wz-CoS was the majority product, but Co_9S_8 was also present. For the rods, Co_9S_8 was the exclusive product, with no evidence of wz-CoS. The data in Figure 3 reveal a morphology dependence to the cobalt sulfide phase that is formed upon cation exchange of roxbyite $Cu_{1.8}S$.

Figure 3 also shows HRTEM images of the Co–S products at 70 ºC. For the plates, lattice spacings of 3.2 and 2.2 Å are consistent with the (100) and (102) planes of wz-CoS. For the spheres, HRTEM images captured particles of wz-CoS and Co_9S_8, which were both observed by XRD. The observed lattice spacing of 5.7 Å for the Co_9S_8 spheres and rods corresponds to the (111) plane of Co_9S_8.

XRD data for the cation exchange reactions carried out at different temperatures are shown in Figures 4a and S2-S4. For the plates, Co_9S_8 begins to form when cation exchange is carried out at temperatures above 70 ºC, although wz-CoS remains the majority phase. The mixture of wz-CoS and Co_9S_8 that was present in the spheres at 70 ºC is also observed at higher reaction temperatures, although Co_9S_8 becomes the majority phase as temperature increases. The rods, which formed exclusively Co_9S_8 at 70 ºC, also form exclusively Co_9S_8 at higher temperatures. Higher temperature therefore favors Co_9S_8, although the temperature dependence of phase evolution is different for each morphology.

In a separate set of experiments, Co-S plates, spheres, and rods were first made by cation exchange at 70 ºC and then afterwards heated in solution with the reaction mixture to 140 ºC. Here, we wanted to see if the phases that formed at 70 ºC changed to Co_9S_8, the thermodynamically favored phase, upon annealing. The XRD data in Figure 4b show that annealing did not change the phases or the phase fractions. The phase(s) formed by cation exchange at 70 ºC were "locked in" and could not be modified, suggesting that the temperature evolution of phase selectivity originated during the cation exchange process rather than as a result of equilibration with the reaction environment at each temperature.

We can now rationalize the data described above in the context of the cation exchange reactions that led to the formation of wz-CoS vs Co_9S_8, as well as the underlying reasons that morphology-dependent phase selectivity was observed. First, wz-CoS and Co_9S_8 both form *concomitant with* cation exchange. When wz-CoS forms first through cation exchange, it cannot subsequently be transformed into the thermodynamically-favorable Co_9S_8 phase upon annealing in solution under conditions identical to those that produce Co_9S_8 upon cation exchange. Second, wz-CoS and Co_9S_8 both form *through* cation exchange. Wz-CoS has not been reported as colloidal nanoparticles made through any method other than cation exchange, and the direct synthesis of colloidal Co_9S_8 nanoparticles is known to require higher temperatures to form.[22–24] Furthermore, morphological retention is a hallmark of cation exchange[3–4], and the ability to access all three shapes would be highly unlikely through identical direct-synthesis methods.

To understand and rationalize the phase selectivity that is observed, we must consider how the cation exchange process differs for different morphologies and temperatures. Wz-CoS forms exclusively (for the plates) or predominantly (for the spheres) at lower temperatures, while Co_9S_8 begins to form at higher temperatures. This makes sense, because Co_9S_8 is the thermodynamically preferred ~1:1 phase of cobalt sulfide.[19] Also, as temperature increases, the solution environment, which contains TOP and oleylamine, becomes more reducing and helps to facilitate formation of the slightly reduced cobalt oxidation state in Co_9S_8 relative to wz-CoS.[25–26]

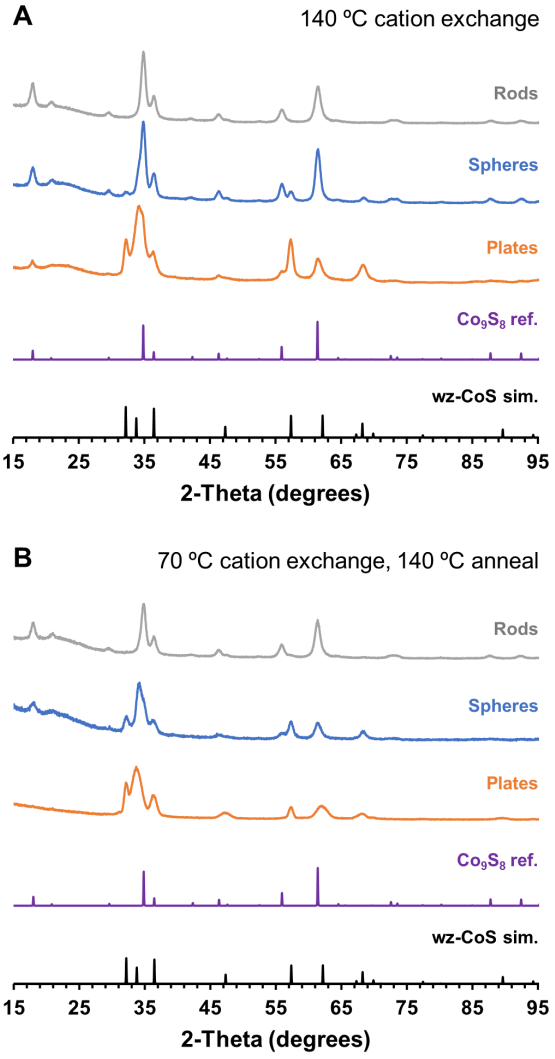

Figure 4. XRD patterns for (A) the products of Co^{2+} exchange of $Cu_{1.8}S$ plates, spheres, and rods at 140 ºC, along with reference patterns for wz-CoS[10] for Co_9S_8 (PDF 04-006-5681) and (B) exchange at 70 °C followed by annealing at 140 °C.

Next, we must consider how the distorted hcp sulfur sublattice of $Cu_{1.8}S$ rearranges to the distorted ccp sulfur sublattice of Co_9S_8. (Note that roxbyite can transform *in situ* to other related $Cu_{2-x}S$ phases that have nearly identical compositions and structures and, most importantly, hcp anion sublattices;[27] see Supporting Information for details.) To rearrange from hcp to ccp, the stacking sequence of the close-packed sulfur layers must shift from ABAB to ABCABC. This shift requires significant lateral movement, when one considers the correlations among all the close-packed planes in the structure (Figure 5). Higher temperatures will help with this process, as the

increased thermal energy will facilitate greater motion and allow the planes to shift more readily. The shifting of close-packed planes during cation exchange has been observed when replacing the Cu^+ cations of roxbyite $Cu_{1.8}S$ nanorods with Zn^{2+} to form ZnS.[28] Here, anion shifting results in the formation of hcp/ccp stacking faults, producing ZnS nanorods containing intermingled regions of wurtzite and zincblende. Stacking fault density, which involves greater anion sublattice shifting, increased with increasing temperature due to increased thermal motion. The same anion shifting that allows a high density of stacking faults to form during cation exchange in ZnS, particularly at higher temperatures, can facilitate the stacking sequence shift that is needed to transform hcp $Cu_{1.8}S$ to ccp Co_9S_8.

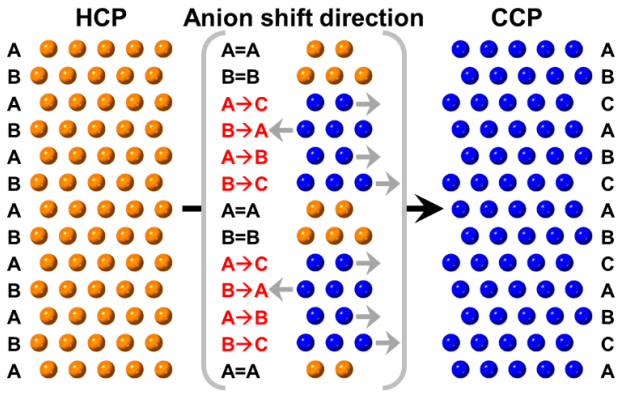

Figure 5. Schematic showing the transition from hcp to ccp, highlighting the various directions that each close-packed plane must shift to accommodate.

We now turn to the morphology dependence of this process. In ZnS, wz-ZnS (hcp) is the favored polymorph at small sizes due to surface energetics,[29–30] as well as the ability of the close packed planes to shift to accommodate at diameters below ~22 nm.[31–32] At larger sizes, zincblende ZnS (ccp) becomes favored.[29] Considering the three morphologies studied here, a key difference is the dimension in the crystallographic direction that the close-packed planes stack – not the aspect ratio, but the number of stacked close-packed planes. The plates contain only ~16 close-packed planes and the entire particle size falls within the expected stability window for hcp, consistent with the formation of wz-CoS. For the spheres, which approach the expected hcp stability limit and consist of ~47 close-packed planes, we observe mostly (although not exclusively) wurtzite CoS at lower temperatures. For the rods, which are much longer in the stacking direction (~140 close-packed planes), ccp is expected to be favored, by analogy to ZnS. Accordingly, the rods would be most susceptible to anion rearrangement. For ZnS, this manifests as hcp/ccp stacking fault formation, since no other compounds could form based on the Zn–S phase diagram, whereas for CoS, it manifests as a shift from wz-CoS (hcp) to Co_9S_8 (ccp). If wz-CoS forms first, the sulfur sublattice structure is "locked in" and the close-packed planes cannot shift because interstitial Co^{2+} holds them together; they can only shift concomitant with cation exchange, while cation migration is in progress and the structure is being locally disrupted. Additional considerations, including the energies of different facets, could also play a role in stabilizing a particular phase.[33]

To help validate the rationale provided above while also considering a system other than Co-S, we show in Figure S6 the ZnS products formed from Zn^{2+} exchange of roxbyite plates, spheres, and rods. There is no evidence for hcp/ccp stacking faults in the wz-ZnS plates, while a small number of stacking faults are present in the ZnS spheres. In the ZnS rods, the density of stacking faults is high. Because the same thermal motion that results in anion sublattice shifting to form stacking faults in ZnS is required to rearrange from hcp to ccp, these observations for the ZnS system qualitatively agree with the phase selectivity observed for the Co–S system.

We have shown that phase selectivity during cation exchange of roxbyite $Cu_{1.8}S$ to form wz-CoS (hcp) vs Co_9S_8 (ccp) is dependent on nanoparticle morphology. The morphology-dependent phase selectivity, which correlates with the number of stacked close-packed planes, is driven by the ability of the close-packed planes to shift laterally during cation exchange, in analogy to hcp/ccp stacking fault formation that is observed in ZnS. This provides a unique pathway for achieving phase control and adds to the growing toolbox of capabilities for rationally designing complex nanostructures using cation exchange reactions. Using these guidelines, it should be possible to design morphologically identical nanoparticles of compositionally and structurally different compounds in the same phase diagram, as well as regions of heterostructured nanoparticles having different compositions and crystal structures.

ASSOCIATED CONTENT

Supporting Information

The Supporting Information is available free of charge on the ACS Publications website.

Complete experimental details and additional XRD and TEM data (PDF)

AUTHOR INFORMATION

Corresponding Author

* res20@psu.edu

Author Contributions

‡ These authors contributed equally.

ACKNOWLEDGMENT

This work was supported by the U.S. National Science Foundation under grant DMR-1904122. TEM and XRD data were acquired at the Materials Characterization Lab of the Penn State Materials Research Institute.

REFERENCES

1. Son, D. H.; Hughes, S. M.; Yin, Y.; Paul Alivisatos, A., Cation Exchange Reactions in Ionic Nanocrystals. *Science* **2004**, *306*, 1009–1012.

2. Beberwyck, B. J.; Alivisatos, A. P., Ion Exchange Synthesis of III–V Nanocrystals. *J. Am. Chem. Soc.* **2012**, *134*, 19977–19980.

3. Beberwyck, B. J.; Surendranath, Y.; Alivisatos, A. P., Cation Exchange: A Versatile Tool for Nanomaterials Synthesis. *The J. Phys. Chem. C* **2013**, *117*, 19759–19770.

4. De Trizio, L.; Manna, L., Forging Colloidal Nanostructures via Cation Exchange Reactions. *Chem. Rev.* **2016**, *116*, 10852–10887.

5. Ha, D.-H.; Caldwell, A. H.; Ward, M. J.; Honrao, S.; Mathew, K.; Hovden, R.; Koker, M. K. A.; Muller, D. A.; Hennig, R. G.; Robinson, R. D., Solid–Solid Phase Transformations Induced through Cation Exchange and Strain in 2D Heterostructured Copper Sulfide Nanocrystals. *Nano Lett.* **2014**, *14*, 7090–7099.

6. Fenton, J. L.; Steimle, B. C.; Schaak, R. E., Tunable intraparticle frameworks for creating complex heterostructured nanoparticle libraries. *Science* **2018**, *360*, 513–517.

7. Fenton, J. L.; Steimle, B. C.; Schaak, R. E., Structure-Selective Synthesis of Wurtzite and Zincblende ZnS, CdS, and $CuInS_2$ Using Nanoparticle Cation Exchange Reactions. *Inorganic Chemistry* **2019**, 58, 672–678

8. Butterfield, A. G.; Steimle, B. C.; Schaak, R. E., Retrosynthetic Design of Morphologically Complex Metal Sulfide Nanoparticles Using Sequential Partial Cation Exchange and Chemical Etching. *ACS Materials Lett.* **2020**, *2*, 1106–1114.

9. Li, H.; Zanella, M.; Genovese, A.; Povia, M.; Falqui, A.; Giannini, C.; Manna, L., Sequential Cation Exchange in Nanocrystals: Preservation of Crystal Phase and Formation of Metastable Phases. *Nano Lett.* **2011**, *11*, 4964–4970.

10. Powell, A. E.; Hodges, J. M.; Schaak, R. E., Preserving Both Anion and Cation Sublattice Features during a Nanocrystal Cation-Exchange Reaction: Synthesis of Metastable Wurtzite-Type CoS and MnS. *J. Am. Chem. Soc.* **2016**, *138*, 471–474.

11. Wark, S. E.; Hsia, C.-H.; Son, D. H., Effects of Ion Solvation and Volume Change of Reaction on the Equilibrium and Morphology in Cation-Exchange Reaction of Nanocrystals. *J. Am. Chem. Soc.* **2008**, *130*, 9550–9555.

12. Lesnyak, V.; Brescia, R.; Messina, G. C.; Manna, L., Cu Vacancies Boost Cation Exchange Reactions in Copper Selenide Nanocrystals. *J. Am. Chem. Soc.* **2015**, *137*, 9315–9323.

13. Gariano, G.; Lesnyak, V.; Brescia, R.; Bertoni, G.; Dang, Z.; Gaspari, R.; De Trizio, L.; Manna, L., Role of the Crystal Structure in Cation Exchange Reactions Involving Colloidal Cu_2Se Nanocrystals. *J. Am. Chem. Soc.* **2017**, *139*, 9583–9590.

14. Hernández-Pagán, E. A.; O'Hara, A.; Arrowood, S. L.; McBride, J. R.; Rhodes, J. M.; Pantelides, S. T.; Macdonald, J. E., Transformation of the Anion Sublattice in the Cation-Exchange Synthesis of Au_2S from $Cu_{2-x}S$ Nanocrystals. *Chem. Mater.* **2018**, *30*, 8843–8851.

15. Li, H.; Brescia, R.; Povia, M.; Prato, M.; Bertoni, G.; Manna, L.; Moreels, I., Synthesis of Uniform Disk-Shaped Copper Telluride Nanocrystals and Cation Exchange to Cadmium Telluride Quantum Disks with Stable Red Emission. *J. Am. Chem. Soc.* **2013**, *135*, 12270–12278.

16. Le, H. K. D.; Xiong, H.; Page, B. A.; Garcia-Herrera, L. F.; McAllister, H. P.; Li, B. C.; Wang, H.; Plass, K. E., Effects of I_2 on $Cu_{2-x}S$ Nanoparticles: Enabling Cation Exchange but Complicating Plasmonics. *ACS Materials Lett.* **2020**, *2*, 140–146.

17. Sharp, C. G.; Leach, A. D. P.; Macdonald, J. E., Tolman's Electronic Parameter of the Ligand Predicts Phase in the Cation Exchange to $CuFeS_2$ Nanoparticles. *Nano Lett.* **2020**, *20*, 8556–8562.

18. Steimle, B. C.; Lord, R. W.; Schaak, R. E., Phosphine-Induced Phase Transition in Copper Sulfide Nanoparticles Prior to Initiation of a Cation Exchange Reaction. *J. Am. Chem. Soc.* **2020**, *142*, 13345–13349.

19. Rao, C. N. R.; Pisharody, K. P. R., Transition metal sulfides. *Prog. Solid State Chem.* **1976**, *10*, 207–270.

20. Geller, S., Refinement of the crystal structure of Co_9S_8. *Acta Crystallogr.* **1962**, *15*, 1195–1198.

21. Steimle, B. C.; Fenton, J. L.; Schaak, R. E., Rational construction of a scalable heterostructured nanorod megalibrary. *Science* **2020**, *367*, 418–424.

22. Maneeprakorn, W.; Malik, M. A.; O'Brien, P., The preparation of cobalt phosphide and cobalt chalcogenide (CoX, X = S, Se) nanoparticles from single source precursors. *J. Mater. Chem.* **2010**, *20*, 2329–2335.

23. Wang, J.; Liu, H.; Liu, Y.; Wang, W.; Sun, Q.; Wang, X.; Zhao, X.; Hu, H.; Wu, M., Sulfur bridges between Co_9S_8 nanoparticles and carbon nanotubes enabling robust oxygen electrocatalysis. *Carbon* **2019**, *144*, 259–268.

24. Mujtaba, J.; He, L.; Zhu, H.; Xiao, Z.; Huang, G.; Solovev, A. A.; Mei, Y., Co_9S_8 Nanoparticles for Hydrogen Evolution. *ACS Appl. Nano Mater.* **2021**, *4*, 1776–1785.

25. Nam, K. M.; Shim, J. H.; Ki, H.; Choi, S.-I.; Lee, G.; Jang, J. K.; Jo, Y.; Jung, M.-H.; Song, H.; Park, J. T., Single-Crystalline Hollow Face-Centered-Cubic Cobalt Nanoparticles from Solid Face-Centered-Cubic Cobalt Oxide Nanoparticles. *Angew. Chem., Int. Ed.* **2008**, *47*, 9504–9508.

26. Carenco, S.; Boissière, C.; Nicole, L.; Sanchez, C.; Le Floch, P.; Mézailles, N., Controlled Design of Size-Tunable Monodisperse Nickel Nanoparticles. *Chem. Mater.* **2010**, *22*, 1340–1349.

27. Nelson, A.; Ha, D.-H.; Robinson, R. D., Selective Etching of Copper Sulfide Nanoparticles and Heterostructures through Sulfur Abstraction: Phase Transformations and Optical Properties. *Chem. Mater.* **2016**, *28*, 8530-8541.

28. Butterfield, A. G.; Alameda, L. T.; Schaak, R. E., Emergence and Control of Stacking Fault Formation during Nanoparticle Cation Exchange Reactions. *J. Am. Chem. Soc.* **2021**, *143*, 1779–1783.

29. Wang, Z.; Daemen, L. L.; Zhao, Y.; Zha, C. S.; Downs, R. T.; Wang, X.; Wang, Z. L.; Hemley, R. J., Morphology-tuned wurtzite-type ZnS nanobelts. *Nat. Mater.* **2005**, *4*, 922–927.

30. Tiwary, C. S.; Srivastava, C.; Kumbhakar, P., Onset of sphalerite to wurtzite transformation in ZnS nanoparticles. *J. Appl. Phys.* **2011**, *110*, 034908.

31. Huang, F.; Banfield, J. F., Size-Dependent Phase Transformation Kinetics in Nanocrystalline ZnS. *J. Am. Chem. Soc.* **2005**, *127*, 4523–4529.

32. Mardix, S., Polytypism: A controlled thermodynamic phenomenon. *Phys. Rev. B: Condens. Matter Mater. Phys.* **1986**, *33*, 8677–8684.

33. Xu, Y.-N.; Ching, W. Y., Electronic, optical, and structural properties of some wurtzite crystals. *Phys. Rev. B* **1993**, 48, 4335–4351.

Insert Table of Contents artwork